

Turbulent jet flow noise prediction.

Peter Moore, Harmen Slot and Bendiks Jan Boersma
 Technical University of Delft
 Laboratory for Aero and Hydrodynamics
 Leeghwaterstraat 21, 2628CA, Delft
 The Netherlands
 p.moore@wbmt.tudelft.nl

Abstract: The text of the abstract follows. In this paper we describe a numerical approach to completely determine the structure of a low Reynolds number compressible jet flow and to compute the associated sound waves in the far field. The method is applied to simulate a Reynolds number 4,000, Mach number 0.8 jet, with the results validated by comparison with the jet reproduced experimentally. The mean flow and far field sound results are shown to while matching conditions are created experimentally inside a low pressure tank. The mean flow results of the DNS are seen to correspond well with our experimental results, and to be compatible with those published in the literature. The semi-analytically obtained sound field is shown to be identical to that obtained purely by the DNS in the near field, while in the far field matches those obtained by us experimentally, and compatible with experimental results previously published.

1 Introduction

Noise prediction has been studied actively since the early 1950's, coinciding with the development of the modern aviation industry and the theoretical basic for flow produced sound provided by Lighthill's Acoustic Analog [7]. Lighthill's theory follows from the observation that the generation and propagation of sound is governed by the Navier-Stokes equations. Simply put, Lighthill rearranged the Navier Stokes equations of fluid flow to the following form:

$$\frac{\partial^2 \rho'}{\partial t^2} - c_\infty^2 \frac{\partial^2 \rho'}{\partial x_i \partial x_i} = \frac{\partial^2 T_{ij}}{\partial x_j \partial x_i} \quad (1)$$

where ρ' is the acoustic density perturbation, c_∞ the ambient speed of sound and T_{ij} the so-called Lighthill stress tensor. This stress tensor is given by

$$T_{ij} = \rho u_i u_j + \mu \left(\frac{\partial u_i}{\partial x_j} + \frac{\partial u_j}{\partial x_i} \right) + (p' - c^2 \rho') \delta_{ij}. \quad (2)$$

where ρ is the fluids density, u_i the fluids velocity, μ the dynamic viscosity of the fluid, p' the acoustic pressure fluctuation and δ_{ij} the Kronecker delta function. Through the rearrangement of terms in the Navier-Stokes equations, Lighthill identifies the possible mechanisms of wave propagation (left hand side of equation (1)) and wave creation with the observation that the right hand side is a perturbation from rest state must represent a source term at least when the perturbation is small. Early noise studies focused on deriving empirical relationships (such as Lighthill's

eight power law which states that the acoustic power radiated by a jet is proportional to the eighth power of the jet speed), using various assumptions to reduce the complexity of the relations studied.

Since this period, the rise of computers has also made possible more sophisticated predictions through solution of the Navier-Stokes equations, albeit with certain simplifying assumptions. Even today with modern computing power, complete solutions of the Navier-Stokes equations are not possible at interesting Reynolds numbers (10^6) or complicated flow geometries, and will not be even for many years to come. However through the use of Direct Numerical Simulation (DNS) it is possible to simulate flows with Reynold's numbers (10^3). While such flows are not found in industrial applications, many feature resemble those of the higher Reynold's number flows. In particular, noise creation mechanisms are believed to be similar in both cases [6], and studying accurately low Reynolds number flows can lead to implications for models of the sound source at higher Reynold's numbers.

In this paper we will use the DNS method developed by [2] to obtain the complete flow and acoustic field of a Reynold's number 4,000, Mach number 0.8 jet for the source region. Through the use of a continuation method (of which Lighthill's Acoustic Analogy is one) we extend the acoustic field to arbitrary locations in the far field. Simultaneously we have constructed an experimental setup that reproduces the jets low Reynold's number, high (but subsonic) Mach number inside the lab, and take simultaneous mea-

measurements of jet flow and acoustic properties. The results of the experiment are used for validation of the numerical results. It is envisaged that complete DNS data will allow in the future a detailed look at the sound creation mechanisms inside turbulent flow.

2 Geometry, governing equations and numerical procedure

In this section we discuss the numerical method used to solve the Navier-Stokes equations. This method was developed to be able to solve fully compressible and turbulent flows, so long as no strong shocks are present. The intended application in this study is to model a high speed (but subsonic) flow with a low (but turbulent) Reynolds number. Such flows are not in general of practical interest, where in the real world, noise creating jets (such as the jet engine of an airplane) have a much higher Reynolds number. Nevertheless many similarities of the jet properties exist between our chosen case and real world jets, and our chosen jet has the decidedly useful advantage of being fully numerically solvable. To model a jet specifically, the boundary conditions are formulated explicitly for this case while the discretization for the interior of the domain remains applicable to more general flows. In

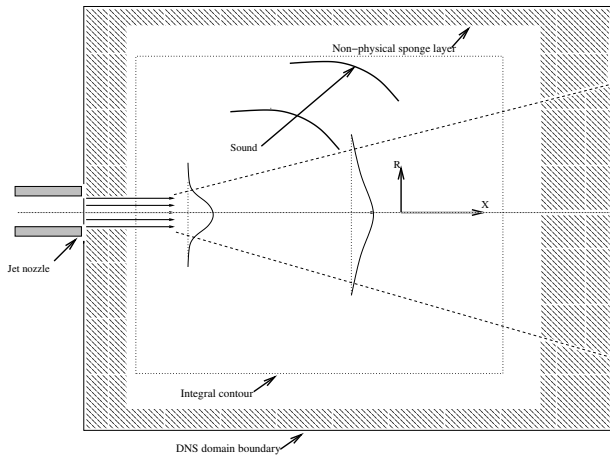


Figure 1: A sketch of the the geometry

figure 1 we show a sketch of the jet geometry. Air is flowing through a cylindrical nozzle with diameter D and velocity U . Downstream of the nozzle the air flow becomes turbulent and the jet spreading becomes linear. The particular case to be studied is a Reynolds number 4,000, Mach number 0.8 flow. At this Mach number, compressibility effects become important. The flow is thus governed by the compressible equations for conservation of mass, momentum and energy, see for instance [5]. The equation for con-

servation of mass reads:

$$\frac{\partial \rho}{\partial t} + \frac{\partial}{\partial x_i} \rho u_i = 0. \quad (3)$$

In which ρ is the fluids density and u_i the velocity vector. The equation for conservation of momentum reads:

$$\frac{\partial \rho u_i}{\partial t} + \frac{\partial}{\partial x_j} [\rho u_i u_j + p] = \frac{\partial}{\partial x_j} \tau_{ij} \quad (4)$$

In which p is the pressure and τ_{ij} the viscous stress tensor. Here we will consider Newtonian flows only and the components of the stress tensor can be written as:

$$\tau_{ij} = \mu \left(\frac{\partial u_i}{\partial x_j} + \frac{\partial u_j}{\partial x_i} - \frac{2}{3} \delta_{ij} \frac{\partial u_k}{\partial x_k} \right)$$

Where μ is the dynamic viscosity of the fluid. Which is in the present study assumed to be constant. The governing equation for the total energy E which is the sum of the internal energy $\rho C_v T$ and the kinetic energy $\rho u_i u_i / 2$ reads:

$$\frac{\partial E}{\partial t} + \frac{\partial}{\partial x_j} (u_j + p)E = \frac{\partial}{\partial x_i} \kappa \frac{\partial T}{\partial x_i} + \frac{\partial}{\partial x_j} u_i \tau_{ij} \quad (5)$$

In which $E = \rho C_v T + \rho u_i u_i / 2$ is the total energy, κ the thermal diffusion coefficient. The thermodynamic quantities P , ρ and T are related to each other by the equation of state for an ideal gas

$$P = \rho R T$$

where R is the gas constant. The speed of sound is defined as:

$$c^2 = \left(\frac{\partial P}{\partial \rho} \right)_S.$$

For an ideal gas it follows that $c = \sqrt{\gamma R T}$ where γ is the specific heat ratio. For an ideal gas the speed of sound is thus only a function of the temperature and of the composition of the gas and independent of the density and pressure!

All the variables in the equations given above are made non-dimensional using the ambient speed of sound c_∞ as reference velocity scale, the ambient density ρ_∞ as reference density, $\rho_\infty c_\infty^2$ as reference pressure, c_∞^2 / C_p as reference temperature, and ambient values for the chemical species. The resulting important non-dimensional numbers are the Reynolds, and Mach number.

$$Re = \frac{\rho_\infty c_\infty D}{\mu}$$

$$Ma = \frac{u}{c_\infty}$$

The Reynolds number given above is a direct result of the non-dimensionalization and is not a very useful number because it is based on the constant acoustic speed c . In the remaining part of this paper we will use the following definition for the Reynolds number

$$Re = \frac{\rho_{\infty} c_{\infty} D}{\mu} \cdot Ma = \frac{\rho_{\infty} u D}{\mu}$$

The numerical method we use is similar to the one used by us before [2]. A staggered formulation has been used. The scalar quantities are stored at the cell centers and the velocity components are stored at the cell faces. All the derivatives are calculated with the following compact finite difference formulation

$$a(f'_{i+1} + f'_{i-1}) + f'_i = \frac{b}{\Delta X}(f_{i+1/2} - f_{i-1/2}) + \frac{c}{\Delta X}(f_{i+3/2} - f_{i-3/2}) + \frac{d}{\Delta X}(f_{i+5/2} - f_{i-5/2}) + \frac{e}{\Delta X}(f_{i+7/2} - f_{i-7/2}) \quad (6)$$

In which f'_i is derivative of f with respect to X in point i and ΔX is the grid spacing. The coefficients in the equation above are obtained by Taylor expansions around grid point i . With the five coefficients a, b, c, d and e in equation (6) we can obtain an 10th order accurate formulation. The values for a, b, c, d and e for this 10th order scheme are (obtained with the Maple Software package):

$$a = 49/190, b = 12985/14592, c = 78841/364800 \\ d = -343/72960, e = 129/851200$$

For the interpolation between various grid locations we use the following formula

$$f_i + a(f_{i+1} + f_{i-1}) = b(f_{i+1/2} + f_{i-1/2}) + c(f_{i+3/2} + f_{i-3/2}) + d(f_{i+5/2} + f_{i-5/2}) + e(f_{i+7/2} + f_{i-7/2}) \quad (7)$$

In the interior we require again 10th order accuracy resulting in the following values for the coefficients a, b, c, d and e (again obtained with the Maple Software package):

$$a = 7/18, b = 1225/1536, c = 49/512, \\ d = -7/1536, e = 1/4608$$

Both formulations are 10th order accurate in space. Close to the boundaries of the domain the order of the scheme has to be reduced. The exact procedure for this is given in [2].

The time integration of the governing equations has been performed with a standard fourth order Runge-Kutta method, with a fixed time step $\Delta t = c_{\infty}/100$. The Courant number used in the simulations is approximately 0.7.

2.1 Boundary conditions

The formulation of boundary conditions for aeroacoustic calculations are extremely important. At the in and outflow boundary of the computational domain we add in a small layer an artificial convection velocity U to the equations (3, 4, 5). Here we demonstrate this procedure for the equation of conservation of mass(3).

$$\frac{\partial \rho}{\partial t} + \frac{\partial}{\partial x}(u + U)\rho - \rho \frac{\partial U}{\partial x} = 0 \quad (8)$$

where U is the artificial convection velocity. In a very small region close to the in and outflow U is set to a value $U > c$ and smoothly reduced to zero in the interior of the domain. With this modification the flow is locally supersonic. This means that at the inflow we can specify velocity, density and total energy as explicit boundary conditions. At the outflow no conditions have to be imposed, due to the local supersonic nature of the equations. As mentioned before in the interior of the computational domain the artificial convection velocity is zero.

In addition to artificial convection, we implement anechoic boundary conditions. Standard boundary conditions for compressible flow, see for instance Thompson [13] and Poinot & Lele [10] will always generate some small reflections. These reflections will have no significant influence on the flow field, but will in general have a quite large influence on the acoustic field, which has by definition a very small amplitude. To implement anechoic conditions, in a layer surrounding the computational domain additional terms are added to equations (3, 4 5) to damp reflections by forcing all the flow variables to their reference states through this layer. Because the lateral boundaries are positioned far away this should not effect the physically interesting region of the flow. Wenn applied to the the conservation of mass equation (3) for example, this takes the form

$$-A(x, y, z)(\rho - \rho_{target}) \quad (9)$$

where ρ is the regular density as appearing in all the equation $A(x, y, z)$ is a function which is zero in the in the interior of the computational domain and has small positive values in the damping layer. ρ_{target} is the time averaged (running average) density obtained from the simulations.

3 Acoustic field continuation

The Ffowcs Williams and Hawkins formulation [15] gives the general result for a sound field radiated by turbulence in the presence of arbitrarily moving surfaces. As pointed out in the original paper [15], and

later by Francescantonio [3] the results can be applied to jet flow by using stationary virtual surfaces. One of the interesting features of this theory is that there are no assumptions made about the nature of the sound source, as opposed to solutions based on Lighthill’s acoustic analogy [7]. In addition, storage requirements remain tractable when the the source is not acoustically compact. as

$$p = \frac{1}{4\pi} \left(\frac{\partial}{\partial t} \int_s \left[\frac{\rho_\infty U_n}{r} \right]_{\text{ret}} dS + \frac{1}{c_\infty} \frac{\partial}{\partial t} \int_s \left[\frac{L_r}{r} \right]_{\text{ret}} dS + \int_s \left[\frac{L_r}{r^2} \right]_{\text{ret}} dS \right) \quad (10)$$

where s is some surface surrounding the flow, u_i and u_n are flow velocities, ρ is density, p is pressure, r is distance from integration point to observer, "ret" denotes evaluation at the retarded time $t' = t - \frac{r}{c_\infty}$, and the subscript 0 represents the mean value of the given quantity. Details of the derivation can be found in [3] and [15]. This integrated form of the equation is obtained using a free space Green function which is almost the only simplification that removes full generality. Because of this, integral surfaces can be placed close to turbulent and/or shear regions provided the nonlinearities there are not too strong.

4 Results

A jet of Reynolds number of 4,000 (based on jet inflow diameter and velocity) and a Mach number of 0.8 (based on jet inflow velocity and c_∞) was simulated using the method described above. Following Uzun *et al* [14], the jet inflow profile is specified as

$$U_{in}(r) = \frac{U_j}{2} \left[1 - \tanh \left(B \frac{r - r_0}{r_0} \right) \right] \quad (11)$$

where $B = 7.5$ is related to the inverse of the initial momentum thickness. No disturbance seeding is done to induce the turbulence, the turbulence was left to develop from Kelvin-Helmholtz instabilities. The computations were performed on a non-uniform Cartesian grid consisting of 200^3 points. The code has been made parallel through the use of the Message Passing Interface (MPI) library. Calculations have been performed on an AMD-Opteron system with 8 CPUs and the simulation required approximately 1 month running time. For the acoustic post-processing, the 2-D Simpsons rule (third order) is used for the integration while time derivatives are calculated using a five point difference method (third order accuracy). To include retarded time effects it was required to first complete the DNS and about 30 gigabytes of data was stored for post-operation.

4.1 Experimental setup

Compressible DNS can only be performed for flows with rather low Reynolds number and high Mach number. To experimentally create a low Reynolds number, high Mach number flow for comparison purposes, we reduce the ambient pressure inside a large steel chamber to a fraction of atmospheric pressure (38 mbars) .through the use of a vacuum pump. The flow into the chamber was controlled by a massflow controller at the inlet and a (controllable) vacuum pump at the outlet of the pressure chamber, and proceeded vertically into the chamber through an 8mm jet nozzle positioned in the chamber floor. Semi-anechoic conditions inside the chamber are created by padding the walls with acoustic dampening material.

Acoustic data is collected from microphones positions on a padded metal arc centered above and pointing towards the jet nozzle. The arc holds 16 microphones at 42 jet diameters from the jet nozzle, equally spaced at angles from 10° to 85° from the jet axis. Data acquisition is performed by two PCI 4472 measurement cards, each capable of simultaneously sampling 8 channels at 100 kHz. A sampling frequency of 65536 Hz was used.

4.2 The directly simulated flow

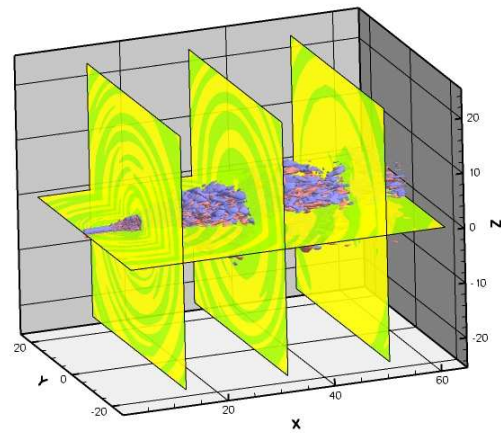


Figure 2: A 3-D isocontour of the vorticity, with red indicating positive vorticity, and blue indicating negative vorticity. 3 vertical slices and 1 horizontal slice of acoustic pressure are also shown.

In this section we give results for the jet obtained numerically and experimentally, and compare with previously published results. In figure 2 we repre-

sent the simulated jet through a contour of vorticity. This picture Just downstream of the nozzle (middle left in the figure) the flow is laminar. A short distance downstream of the jet nozzle there is a transitional region and further downstream the jet becomes fully turbulent and the spreading rate is linear as could be expected from standard turbulence theory. Figure 3

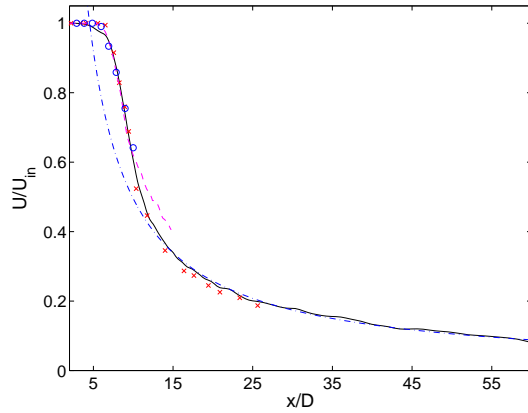


Figure 3: Centerline velocity profiles. Circles are experimental data of Stromberg for Re 3600, Ma 0.83 jet, crosses is our experimental data, full line is our DNS, dash-dotted line is fit of equation (12), and broken line is from DNS of Freund for Re 3600, Ma 0.83 jet.

compares the centerline velocity of our DNS with our experimentally obtained results using a Pitot tube, and with published experimental [11] and numerical [6] results of a Reynolds number 3,600, Mach number 0.8 jet. To obtain figure 3 each jet was shifted until the end of the respective potential core aligned visually with that of the data from Stromberg [11], accounting for differing virtual jet origins. The agreement is very good. The main differences between our experimental data and our DNS can be accounted for by the unreliability of the Pitot tube which ignores the possibility of back flow in low speed regions and the radial motion of the jet near the end of the potential core. Importantly both the DNS and experimental data match reasonably downstream, an indication that the turbulence is accurately being simulated. The decay rates are found by fitting the expected downstream decay profile (12) to each result were B_u of 5.37 and 5.22 for the DNS and for the experimental jet. This is consistent with an expectation of between 5.0 and 5.9 [1]

$$\frac{U_c}{U_{in}} = \frac{B_u}{x - x_0} \quad (12)$$

4.3 The acoustic field

To verify that the FWH predictions are consistent with the aeroacoustic field only by DNS we match acoustic pressure signals in an overlap region where both results are available. For example, figure 4 gives these signals at the point $x = 24.2D_j, y = 15.96D_j, z = 0$. The signals are almost identical, with a small departure due to grid stretching between the integral contour and chosen comparison point. Next the sound

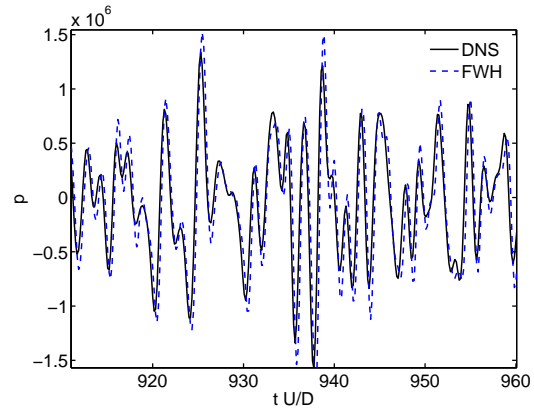


Figure 4: Section of pressure signal at $x = 24.2D_j, y = 15.96D_j$. Full line is directly from DNS, dashed line from FWH formulation.

pressure levels and directivity are compared for our DNS and experimental data again with two jets of Freund [6] and Stromberg [11] in figure 5. Here the

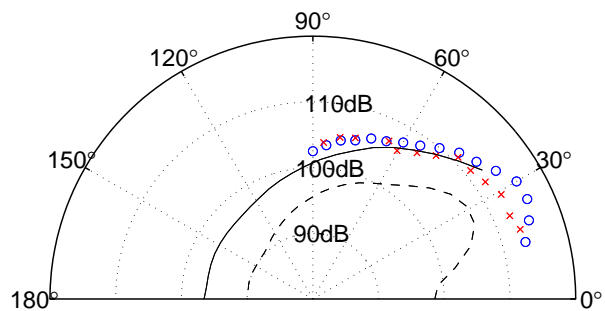


Figure 5: Far field sound pressure levels. Circles are Stromberg's data at $r = 30.0D_j$ for Re 3600, Ma 0.83 jet. Full line is DNS at $r = 30.0D_j$, crosses is our experimental data at $r = 30.0D_j$ (scaled back from $r = 42.0D_j$) and broken line is DNS at $r = 120.0D_j$.

agreement at the radius of $30D_j$ is quite good. The jets of Freund and Stromberg are taken at the slightly higher Mach number of 0.83, which accounts for the 1-2 dB difference in the sound pressure levels while

the difference in Reynolds number is not expected to significantly effect the SPL. The experimental results match well for intermediate angles, but departure at low angles is believed to be caused by reflections inside the tank. Incidentally, the SPL at the radius of $30D_j$ of our DNS data is only shown from an angle of 35° onwards due to limitations imposed by the integral contour boundary. No problem exists at a radius of $120D_j$ and the expected dropping of SPL at angles close to 0° is seen nicely on that curve.

5 Conclusion

A numerical procedure to obtain the complete turbulent flow and sound fields has been outlined and applied to the case of a turbulent jet. The numerical procedure consists of a direct numerical simulation (DNS) code, which solves the Navier-Stokes equations using a high order compact finite difference formulation. For boundary conditions, an artificial convection velocity is added to ensure local supersonic conditions, and artificial damping terms are added to create anechoic conditions. Secondly, to compute far-field sound, we use the Ffowcs Williams and Hawkins method which computes the sound pressure field at arbitrary locations based on knowledge acquired by the DNS of the flow history in the turbulent region. Finally we recreated the same conditions experimentally in the lab for verification purposes. The method was applied to simulate a Reynolds number 4,000, Mach number 0.8 jet and the results compared to our experimental data as well as , previously published experimental and numerical results of a Reynolds number 3,600, Mach number 0.83 jet. The centerline velocity profiles and sound pressure levels of our simulation were consistent with these results. It is hoped that the combination of a complete jet simulation and simultaneous experimental measurements of the flow and acoustics of the same phenomena will allow us to investigate more deeply the underlying mechanisms by which noise is created in turbulent flows.

Acknowledgements: This project was financially supported by the Dutch Technology Foundation STW under grant number DSF:6181

References:

- [1] D.J. Bodony and S.K. Lele. Jet noise prediction of cold and hot subsonic jets using large-eddy simulation. *AIAA Paper*, 3022, 2004.
- [2] B.J. Boersma. A staggered compact finite difference approach for the compressible navier-stokes equations. *J. of Comp. Phys*, 208:675–690, 2005.
- [3] P. Di Francescantonio. A new boundary integral formulation for the prediction of sound radiation. *J. Sound and Vibration*, 202, No. 4:491–509, 1997.
- [4] J. B. Freund. Noise-source turbulence statistics and the noise from a mach 0.9 jet. *Physics of Fluids*, 15, No. 6:1788–1799, 2003.
- [5] M.E. Goldstein. *Aeroacoustics*. McGraw-Hill, New York, 1976.
- [6] Freund. J.B. Noise sources in a low-reynolds-number turbulent jet at mach 0.9. *J. Fluid Mech.*, 438:277–305, 2001.
- [7] M.J. Lighthill. On sound generated aerodynamically, part 1: General theory. *Proc. Roy. Soc. Lon.*, A 211:564–587, 1952.
- [8] P. Moore and B. Boersma. Investigation of the noise from cold and heated subsonic jets. *12th AIAA/CEAS Aeroacoustics Conference*, 2500, 2006.
- [9] P. Moore and B.J. Boersma. Use of surface integral methods in the computation of the acoustic far field of a turbulent jet. *Proceedings of Direct and Large Eddy Simulation 6*, 2005.
- [10] T.J. Poinso and S.K. Lele. J. comp. phys. *Boundary conditions for direct simulation of compressible flows*, 101:104–129, 1992.
- [11] J.L. Stromberg, D.K. Mclaughlin, and T.R.. Troutt. Flow field and acoustic properties of a mach number 0.9 jet at a low reynolds number. *Journal of Sound and Vibration*, 72:159–176, 1980.
- [12] H.K. Tanna. An experimental study of jet noise i: Turbulent mixing noise. *Journal of Sound and Vibration*, 50, No. 3:405–428, 1977.
- [13] K.W. Thompson. Time dependent boundary conditions for hyperbolic systems. *J. Comp. Phys.*, 68:1–24, 1987.
- [14] A. Uzun, G.A. Blaisdell, and A.S. Lyrintzis. Coupling of integral acoustics methods with les for jet noise prediction. *AIAA Paper*, 0517, 2004.
- [15] J.E.F. Williams and D.L. Hawkings. Sound generated by turbulence and surfaces in arbitrary motion. *Proc Roy. Soc. Lon.*, A264:321–342, 1969.